



Identification of peripheral blood immune infiltration signatures and construction of monocyte-associated signatures in ovarian cancer and Alzheimer's disease using single-cell sequencing

Songyun Zhao^a, Bicheng Ye^b, Hao Chi^c, Chao Cheng^{a, **}, Jinhui Liu^{d, *}

^a Department of Neurosurgery, Wuxi People's Hospital Affiliated to Nanjing Medical University, Wuxi, 214000, China

^b School of Clinical Medicine, Yangzhou Polytechnic College, Yangzhou, 225000, China

^c Clinical Medical College, Southwest Medical University, Luzhou, 646000, China

^d Department of Gynecology, The First Affiliated Hospital of Nanjing Medical University, Nanjing, 210000, China

ARTICLE INFO

Keywords:

OC
AD
Single-cell RNA-Seq
Machine learning
Tumor microenvironment
Immunotherapy
Prognostic model

ABSTRACT

Background: Ovarian cancer (OC) is a common tumor of the female reproductive system, while Alzheimer's disease (AD) is a prevalent neurodegenerative disease that primarily affects cognitive function in the elderly. Monocytes are immune cells in the blood that can enter tissues and transform into macrophages, thus participating in immune and inflammatory responses. Overall, monocytes may play an important role in Alzheimer's disease and ovarian cancer.

Methods: The CIBERSORT algorithm results indicate a potential crucial role of monocytes/macrophages in OC and AD. To identify monocyte marker genes, single-cell RNA-seq data of peripheral blood mononuclear cells (PBMCs) from OC and AD patients were analyzed. Enrichment analysis of various cell subpopulations was performed using the "irGSEA" R package. The estimation of cell cycle was conducted with the "tricycle" R package, and intercellular communication networks were analyzed using "CellChat". For 134 monocyte-associated genes (MRGs), bulk RNA-seq data from two diseased tissues were obtained. Cox regression analysis was employed to develop risk models, categorizing patients into high-risk (HR) and low-risk (LR) groups. The model's accuracy was validated using an external GEO cohort. The different risk groups were evaluated in terms of immune cell infiltration, mutational status, signaling pathways, immune checkpoint expression, and immunotherapy. To identify characteristic MRGs in AD, two machine learning algorithms, namely random forest and support vector machine (SVM), were utilized.

Results: Based on Cox regression analysis, a risk model consisting of seven genes was developed in OC, indicating a better prognosis for patients in the LR group. The LR group had a higher tumor mutation burden, immune cell infiltration abundance, and immune checkpoint expression. The results of the TIDE algorithm and the IMvigor210 cohort showed that the LR group was more likely to benefit from immunotherapy. Finally, ZFP36L1 and AP1S2 were identified as characteristic MRGs affecting OC and AD progression.

Conclusion: The risk profile containing seven genes identified in this study may help further guide clinical management and targeted therapy for OC. ZFP36L1 and AP1S2 may serve as biomarkers and new therapeutic targets for patients with OC and AD.

* Corresponding author.

** Corresponding author.

E-mail addresses: 2021122190@stu.njmu.edu.cn (S. Zhao), Mr_chengchao@126.com (C. Cheng), jinhui.liu@njmu.edu.cn (J. Liu).

1. Introduction

Ovarian cancer (OC) is associated with the highest mortality rate among gynecologic cancers, leading to over 100,000 deaths annually in developed regions [1]. Despite advancements in standard care over the past two decades, the survival rate for ovarian cancer has not shown significant improvement [2]. About 60% of ovarian cancer patients are diagnosed at an advanced stage. While some patients initially respond well to surgery and chemotherapy, approximately 70% experience disease recurrence and ultimately succumb to chemoresistance [3,4]. Immunotherapy for ovarian cancer faces significant challenges due to the immunosuppressive state of the tumor microenvironment. Therefore, there is an urgent need to identify effective predictors of immunotherapy response and stratify patients for appropriate management.

AD, an irreversible neurodegenerative disease, is primarily associated with aging. It is characterized by progressive memory loss and cognitive dysfunction. Pathological changes in AD include beta-amyloid deposition, neuronal loss, synaptic dysfunction, and neuroinflammation in the brain [5–7]. In 2021, the United States had around 6.2 million individuals aged 65 years and older affected by AD [8]. However, current clinical management and treatment options for AD are still limited in their effectiveness, necessitating further research into the disease's mechanisms.

In contrast to the excessive neuronal cell death observed in neurodegenerative diseases, such as Alzheimer's disease (AD), cancer is characterized by uncontrolled cell proliferation and a strong resistance to cell death [9]. Interestingly, emerging studies suggest a reciprocal relationship between these two diseases, indicating that patients with neurodegenerative diseases like AD have a lower likelihood of developing cancer [10]. Epidemiological evidence from previous studies consistently demonstrates a decreased incidence of Alzheimer's disease following a cancer diagnosis [11]. Notably, the overexpression of PIN1, a peptidyl-prolyl cis/trans isomerase, has been associated with cancer development, while its absence is linked to the formation of Alzheimer's biomarkers in the brain [12].

While the pathogenesis and treatment of ovarian cancer and Alzheimer's disease differ fundamentally, recent research suggests a potential connection between them. Statistics reveal that women are approximately twice as likely as men to develop Alzheimer's disease [13]. In one study, women who underwent bilateral salpingo-oophorectomy had a higher risk of developing dementia and Parkinson's disease compared to those who underwent conservative treatment [14,15]. This increased risk may be attributed to the treatment of ovarian cancer and oophorectomy, as these procedures can alter estrogen levels, which in turn can affect neuronal survival and function [16,17]. Moreover, there are shared risk factors and biomarkers between ovarian cancer and Alzheimer's disease. For instance, chronic inflammation, metabolic disorders, abnormal blood glucose levels, and abnormal estrogen levels may increase the risk of developing both ovarian cancer and Alzheimer's disease [18,19]. This provides a potential explanation for the association between the two.

In this study, we conducted a comprehensive analysis of the immune microenvironment in ovarian cancer (OC) and Alzheimer's disease (AD) using peripheral blood mononuclear cells (PBMCs) and tissues. We employed the CIBERSORT deconvolution algorithm to compare the immune characteristics of both diseases, focusing on the potential role of monocytes/macrophages in disease progression. Our main objective was to identify and characterize OC patients with distinct monocyte profiles. We integrated bulk sequencing and single-cell RNA sequencing (scRNA-seq) data from OC patients to identify monocyte-associated genes (MRGs) that have a high prognostic value. Additionally, we employed a machine learning approach to identify characteristic MRGs in AD. The findings of this study establish a unique prognostic signature based on MRGs, which can effectively predict the prognosis of OC patients and provide valuable insights for immunotherapy strategies. Furthermore, we identified ZFP36L1 and AP1S2 as key genes that are believed to play significant roles in the progression of both OC and AD. These genes represent potential new targets for the treatment of these diseases.

2. Materials and methods

2.1. Source of raw data

We conducted gene expression data synthesis from the Gene Expression Omnibus (GEO) and The Cancer Genome Atlas (TCGA) databases to obtain ovarian cancer gene expression data measured in fragments per kilobase million (FPKM) and related clinicopathological data. Due to the absence of sequencing data from normal ovarian samples in the TCGA database, we downloaded the merged TCGA-GTEX cohort from the UCSC Xena database. Two GEO cohorts (GSE9891, GSE63885) and the TCGA-OV cohort were also obtained for subsequent analysis. We applied the "sva" algorithm to merge the two GEO datasets and eliminate batch effects [20]. FPKM values were converted to transcripts per kilobase million (TPM), considering TPM to be equivalent to transcripts from the GEO microarray platform [21]. The subsequent prognostic models were constructed using a total of 376 patients from the TCGA cohort, 285 patients from the GSE989 cohort, and 101 patients from the GSE63885 cohort. Additionally, we obtained 10× single-cell RNA sequencing data from two peripheral blood samples of OC patients from GSE213243 [22]. A cohort comprising 20 healthy controls and 48 ovarian cancer patients was sourced from GSE31682 [23].

Furthermore, scRNA-seq data consisting of three peripheral blood samples from Alzheimer's disease (AD) patients were downloaded from GSE181279 [24]. To maintain gender consistency with the OC cohort, a GSE97760 cohort consisting of elderly women was selected, including peripheral blood sequencing data from nine patients with advanced AD and ten age-matched healthy female controls [25]. Finally, cortical sequencing data from the GSE5281 cohort, comprising 37 female patients with AD and 21 female controls, were obtained [26]. All raw GEO datasets were preprocessed using the "affy" package in R, which involved background calibration, normalization, and log₂ transformation [27].

2.2. Processing of single-cell sequencing data

The scRNA-seq data were analyzed using the “Seurat” and “SingleR” R packages [28,29]. To ensure high-quality cellular data, only genes expressed in at least three single cells were included. Cells with fewer than 200 or more than 10,000 genes, fewer than 1000 molecules, and more than 20% of mitochondrial and ribosomal genes were excluded. The “harmony” R package was utilized to remove batch effects between samples [30]. Subsequently, the scRNA-seq data were normalized using the “NormalizeData” function and transformed into Seurat objects. The top 2000 highly variable genes were identified using the “FindVariableFeatures” function. Principal component analysis (PCA) was performed using the “RunPCA” function of the “Seurat” R package to reduce the dimensionality of the scRNA-seq data based on these genes. Significant principal components (PCs) were identified using JackStraw analysis, and appropriate PCs were selected for cell clustering analysis based on the proportion of variance. The integrated data were then clustered using the “FindNeighbors” and “FindClusters” functions, and cell visualization was performed using the UAMP method. To identify genes specifically expressed in each cluster, the “FindAllMarkers” and “FindMarkers” functions of the “scran” R package were employed to conduct Wilcoxon tests between pairs of cell clusters. The expression of specific genes was visualized using the “featureplot” function. Cell types were assigned using the “SingleR” R package [28] and referenced cell type annotations from a previous study [31]. The “irGSEA” R package (<https://github.com/chuiqin/irGSEA/>) was used to score individual cells using a multi-genomic enrichment approach and generate a multi-genomic enrichment scoring matrix. Differential gene expression analysis was performed for each cell subpopulation in the enrichment score matrix using the Wilcoxon test. The “tricycle” R package was utilized to estimate the cell cycle by scoring each cell based on the expression of G2/M [32] and S-phase marker genes. Lastly, the R package “CellChat” [33] was employed to analyze cell-to-cell communication networks, evaluate receptor and ligand expression levels, and infer potential cell-to-cell interactions.

2.3. Calculating risk scores and constructing MRG-related prognostic models in OC

To calculate MRG-related scores and quantify the prognostic information for each OC sample, the following steps were performed. First, univariate Cox regression analysis ($p < 0.05$) was conducted on 134 differentially expressed monocyte-related genes (DEMGRs) that were shared between OC and AD. This analysis identified 13 DEMGRs associated with the prognosis of OC. To create a predictive gene signature associated with MRG-related risk scores in the TCGA training set, stepwise multiple Cox regression analysis was utilized to select candidate genes. The risk score associated with MRG was calculated as follows: $\text{risk score} = \sum(\text{Exp}_i * \text{coef}_i)$, where coef_i and Exp_i represent the expression and risk factors of each gene, respectively. Next, patients in the TCGA training set were divided into low-risk (LR) and high-risk (HR) groups based on the median values of the risk scores. Kaplan-Meier survival analysis [34] was performed for each group to assess the survival differences. Principal component analysis (PCA) was conducted using the “ggplot2” R package. The area under the curve (AUC) was calculated using the “survivalROC” R package to evaluate the predictive performance.

2.4. Correlation enrichment analysis

To analyze the gene ontology (GO) and Kyoto Encyclopedia of Genes and Genomes (KEGG) pathways, we utilized the “clusterProfiler” R package and visualized the results using the “circlize” package. We considered p-values below 0.05 as statistically significant, indicating enrichment of specific pathways [35]. To further investigate the biological functions that differed between the high and low-risk populations, we performed Gene Set Enrichment Analysis (GSEA) using the “c2.cp.kegg.v6.2.symbols.gmts” file from the MsigDB database. Significance was determined based on a threshold of $p < 0.05$ and false discovery rate (FDR) < 0.25 . This analysis helped identify enriched pathways and biological processes associated with the high and low-risk groups. To explore the MRG-related biological functional differences, we conducted genomic variation analysis using the Gene Set Variation Analysis (GSVA) method. For this analysis, we used the “c2.cp.kegg.v6.2.symbols.gmts” file [36]. Additionally, we created customized Gene Matrix Transposed (gmt) files to perform GSEA in the GSE31682 and GSE97760 cohorts. These files were based on the marker genes of each cell identified in the single-cell sequencing data.

2.5. Immunotherapeutic response prediction

TIDE (Tumor Immune Dysfunction and Exclusion) is a computational tool available at <http://tide.dfci.harvard.edu/>. It is designed to assess the likelihood of immune escape in tumor samples by analyzing their gene expression profiles [37]. The tool specifically examines the expression of genes associated with immune escape, including immune checkpoints and antigen presentation machinery. By evaluating these gene expressions, TIDE can predict the probability of tumor immune dysfunction and rejection. In the context of predicting response to immunotherapy, the TIDE tool was utilized in combination with data from the invigor 210 cohort. This cohort consists of patients with locally advanced and metastatic uroepithelial cancer who received *anti*-PD-L1 immunotherapy. By integrating the TIDE analysis with the invigor 210 data, researchers aimed to identify subgroups of patients likely to respond favorably or unfavorably to the immunotherapy treatment [38].

2.6. Tumor microenvironment (TME) and tumor mutational load (TMB)

In order to evaluate the infiltration of immune cells in ovarian cancer patients with distinct survival outcomes, we utilized single-gene set enrichment analysis (ssGSEA). Through this analysis, we were able to assign scores to 28 immune cell types present within the

tumor microenvironment (TME) of both low-risk (LR) and high-risk (HR) patient groups [39]. Additionally, we utilized the “maftools” R package to identify somatic mutations in OC patients from the TCGA database. By analyzing the mutation profiles, we calculated the tumor mutation load (TMB) score for each patient in both the LR and HR groups [40]. The TMB (tumor mutational burden) score quantifies the quantity of somatic mutations detected in the tumor genome, providing insight into genomic instability. Additionally, we utilized the “estimate” package to estimate tumor purity and TME (tumor microenvironment) scores for each patient. Tumor purity refers to the proportion of cancer cells within the tumor sample, while the TME score provides an estimation of the abundance of stromal and immune cells in the tumor microenvironment. These scores enhance our understanding of tumor characteristics and the interactions between cancer cells and the surrounding tissue.

2.7. Selection of characteristic genes

In our study on Alzheimer’s disease (AD), we employed two machine learning algorithms, namely random forest and SVM-RFE, to filter feature genes associated with the disease. To identify the most important genes related to AD, we utilized the random forest algorithm and performed recursive feature elimination (RFE). RFE is a supervised approach that iteratively ranks the importance of genes based on their ability to contribute to the classification of AD. The random forest algorithm evaluated the importance of the feature genes using 10-fold cross-validation, a technique that divides the data into 10 subsets and performs the analysis iteratively, ensuring robustness. Genes with a relative importance value greater than zero were considered as feature genes, indicating their relevance in distinguishing AD [41]. Additionally, we employed SVM-RFE, another machine learning algorithm, to select relevant characteristics and eliminate redundant ones in the context of AD. SVM-RFE utilizes support vector machines (SVM) to rank and select the most informative genes for classification. This method was found to be superior to other approaches in identifying the most relevant genes associated with diseases [42]. By combining these two machine learning algorithms, we aimed to identify a set of feature genes that are crucial for distinguishing AD and provide insights into the underlying molecular mechanisms of the disease.

2.8. Immunohistochemical techniques and quantitative real-time polymerase chain reaction PCR (RT-qPCR)

To evaluate the relative mRNA expression levels of ZFP36L1, AP1S2, and GAPDH as a normalized control, we performed RNA isolation from the ovarian epithelial cell line IOSE, ovarian cancer cell lines SKOV-3 and A2780, as well as tissue samples. Total cellular RNA was extracted using Trizol reagent (Invitrogen), and cDNA synthesis was carried out using SuperScript II reverse transcriptase (Invitrogen) following the manufacturer’s instructions. For quantitative mRNA expression analysis, SYBR Premix Ex TaqII (Takara, Dalian, China) was employed. The primer sequences used for amplification are provided below:

ZFP36L1:

Forward primer: 5'-ACTCCAGCCGCTACAAGAC-3'

Reverse primer: 5'-CGTAGGGGCAAAGCCGAT-3'

AP1S2:

Forward primer: 5'-TTCAGACCGTTTTAGCACGGA-3'

Reverse primer: 5'-TGCCTGATCCTCAATAGCACA-3'

GAPDH:

Forward primer: 5'-GGAGCGAGATCCCTCCAAAAT-3'

Reverse primer: 5'-GGCTGTTGTCATACTTCTCATGG-3'

The SYBR Premix Ex TaqII is a commonly used reagent for quantitative real-time PCR (qPCR), and the primer sequences provided are specific to the target genes ZFP36L1, AP1S2, and GAPDH. These primers allow for the amplification and quantification of the respective mRNA transcripts.

We employed transcriptomic and proteomic methods to investigate RNA and protein expression profiles in various human tissues and organs. The Human Protein Atlas (HPA, <https://www.proteinatlas.org/>) served as the source of data for this study.

2.9. Statistical analyses

All statistical analyses were carried out using R version 4.1.2 along with its corresponding support package. To evaluate prognostic significance and compare patient survival, Kaplan-Meier survival analyses and log-rank tests were performed on different subgroups within each dataset. Student’s t-test was used to determine differences between normally distributed groups, while the Wilcoxon test was employed for non-normally distributed variables. The significance level for all statistical tests was set at $P < 0.05$, indicating that results with a p-value below this threshold were considered statistically significant.

3. Results

3.1. Characterization of the immune microenvironment in OC and AD

In order to find common features of the immune microenvironment and immune function in patients with OC and AD, the CIBERSORT algorithm was first applied to assess the level of infiltration of different types of immune cells in peripheral blood as well as in disease-bearing tissues in OC and AD, respectively. A higher percentage of monocytes in peripheral blood was revealed in patients with OC relative to normal patients (Fig. 1A) through CIBERSORT analysis. Similarly, the level of monocyte infiltration in peripheral

blood was higher in AD patients; however, a statistical difference between the two groups was not observed, probably due to the small sample size. Additionally, low levels of M0 macrophages were found in the peripheral blood of AD patients (Fig. 1C). This seems to indicate that a similar role in the development of both diseases is played by monocytes/macrophages. To further confirm our view, sequencing data from ovarian cancer tissue and cortical tissue from women with Alzheimer's disease were also analyzed using CIBERSORT. Higher levels of M0 and M1 macrophage infiltration in OC tissues compared to normal tissues were identified (Fig. 1B). Similarly, brain tissues of AD patients exhibited higher infiltration levels of M1 macrophages (Fig. 1D). Thus, an important role in ovarian cancer and Alzheimer's disease may be played by macrophages, but further studies are needed to determine their exact role.

3.2. scRNA-seq of peripheral blood from OC patients

Gene expression profile data from peripheral blood of 2 OC patient samples were obtained for further analysis based on scRNA-seq data from GSE213243. After strict quality control filtering, the two samples contained 5464 and 4705 cells, respectively, that were included in the subsequent analysis (Supplementary Fig. 1A). The data was then normalized and batch effects were removed, followed by the selection of the top 2000 highly variable genes (Supplementary Fig. 1B). For dimensionality reduction, the PCA method was employed, and the top 18 PCs were selected based on P values (Supplementary Fig. 1C). Cell subpopulations were annotated using the "singleR" algorithm in combination with a manual annotation approach utilizing marker genes, and UMAP was utilized to visualize specific cell subpopulations (Fig. 2A, Supplementary Fig. 1D). The relative expression of marker genes in each cell subpopulation was depicted in the heatmap (Supplementary Fig. 1E). Results from irGSEA revealed that monocytes in OC patients were predominantly associated with tumor-related pathways, including angiogenesis, inflammatory response, and epithelial-mesenchymal transition (EMT) (Fig. 2B). In terms of the cell cycle, monocytes were mainly clustered in the S and G2 phases (Fig. 2C). Finally, CellChat was employed to assess potential signaling pathways and interactions between different cell subpopulations in the peripheral blood of OC patients. The closest intercellular communication was observed between monocytes and epithelial/tumor cells (Fig. 2D and E), with monocytes primarily influenced by HLA signaling (Fig. 2F).

3.3. scRNA-seq of peripheral blood from AD patients

Meanwhile, gene expression profile data from peripheral blood of 3 AD patient samples were obtained for further analysis based on scRNA-seq data from GSE181279. After filtering out low-quality cells through quality control measures, the subsequent analysis included 585, 681, and 371 cells in the respective samples (Supplementary Fig. 2A). Following the removal of batch effects and data normalization, the top 2000 highly variable genes were selected (Supplementary Fig. 2B). Dimensionality reduction was performed using the PCA method, and the top 17 PCs were chosen for further analysis (Supplementary Fig. 2C). Each cell cluster was annotated using the "singleR" algorithm in combination with known marker genes, and UMAP was utilized to visualize specific cell subpopulations (Fig. 3A, Supplementary Fig. 2D). The heatmap illustrated the relative expression of marker genes in each cell

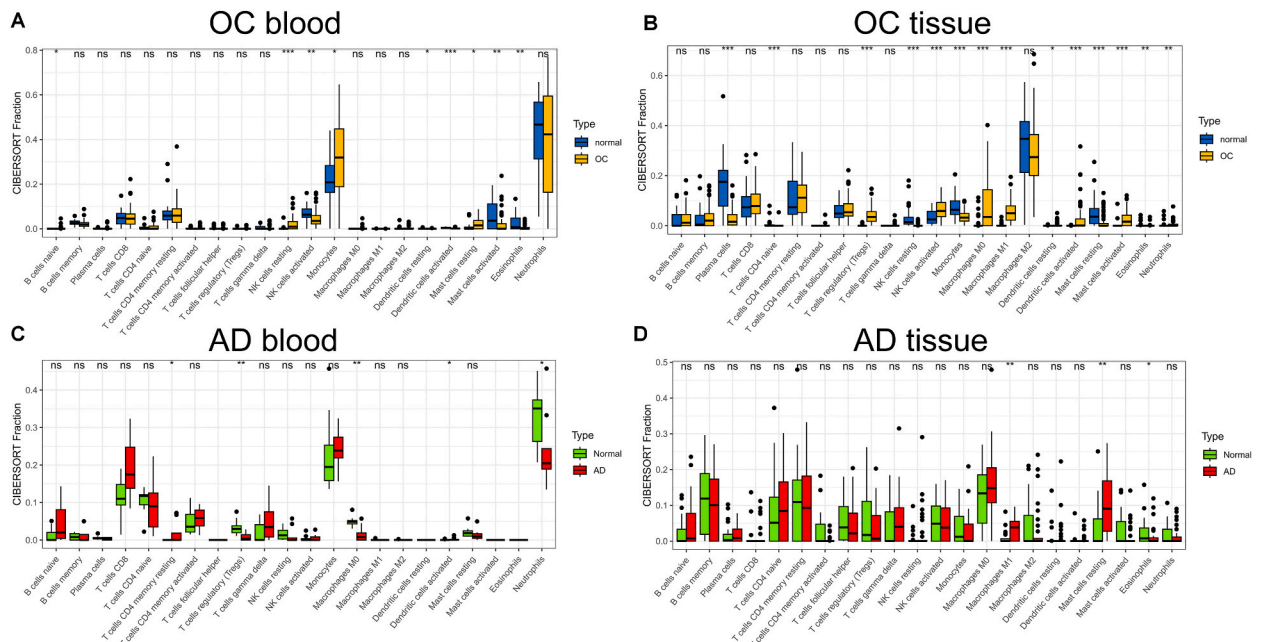


Fig. 1. Comparison of the level of infiltration of 22 immune cells. (A) Peripheral blood of OC and control group. (B) OC and normal control tissue. (C) Peripheral blood of AD and control group. (D) AD and normal control tissue. ns no significance, * $P < 0.05$, ** $P < 0.01$, *** $P < 0.001$, OC, Ovarian cancer; AD, Alzheimer's disease.

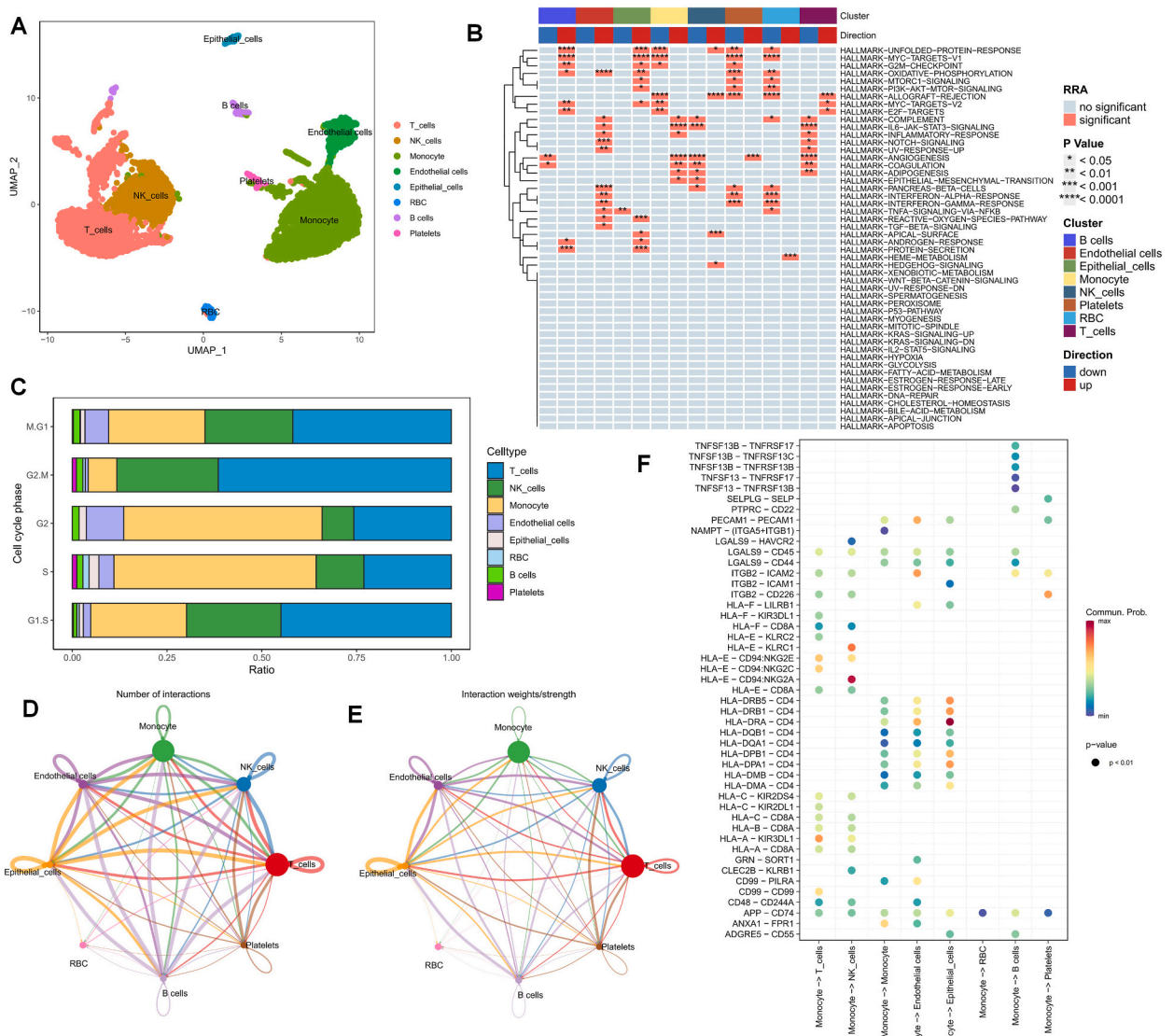


Fig. 2. Classification and analysis of cell subpopulations in the peripheral blood of ovarian cancer patients. **(A)** U-MAP plots of different cell subpopulations by color association. **(B)** GSEA plots showing the terms of the hallmark gene set enrichment pathway for each identified cell subpopulation. **(C)** The number of each cell subpopulation in proportion to the number of different cycles of cell development. **(D, E)** Number and strength of intercellular communication networks inferred by calculating the likelihood of communication, with the thickness of the lines representing strength or number. **(F)** Cellular signals from different cell types to monocytes. The vertical axis shows the interactions between receptors and ligands in selected cell types, with different colors representing the intensity. (For interpretation of the references to color in this figure legend, the reader is referred to the Web version of this article.)

subpopulation (Supplementary Fig. 2E). Interestingly, similar to the findings in OC, monocytes/macrophages in AD patients were predominantly associated with angiogenesis, inflammatory response, and various substance metabolism-related pathways (Fig. 3B). Moreover, in terms of the cell cycle, monocytes exhibited a notable accumulation in the G2 phase (Fig. 3C). CellChat analysis was employed to explore potential signaling pathways and interactions among different cell subsets in the peripheral blood of AD patients. The intensity of intercellular communication was highest between monocytes and NK cells and T cells (Fig. 3D and E), and monocytes were primarily influenced by HLA-related signals (Fig. 3F).

3.4. Monocyte-related genes in ovarian cancer and Alzheimer's disease

Based on the results of scRNA-seq data, we extracted marker genes for various types of cells in OC and AD from peripheral blood. GSEA was performed in both the peripheral blood and tissue cohorts of ovarian cancer, and monocyte-associated pathways were found

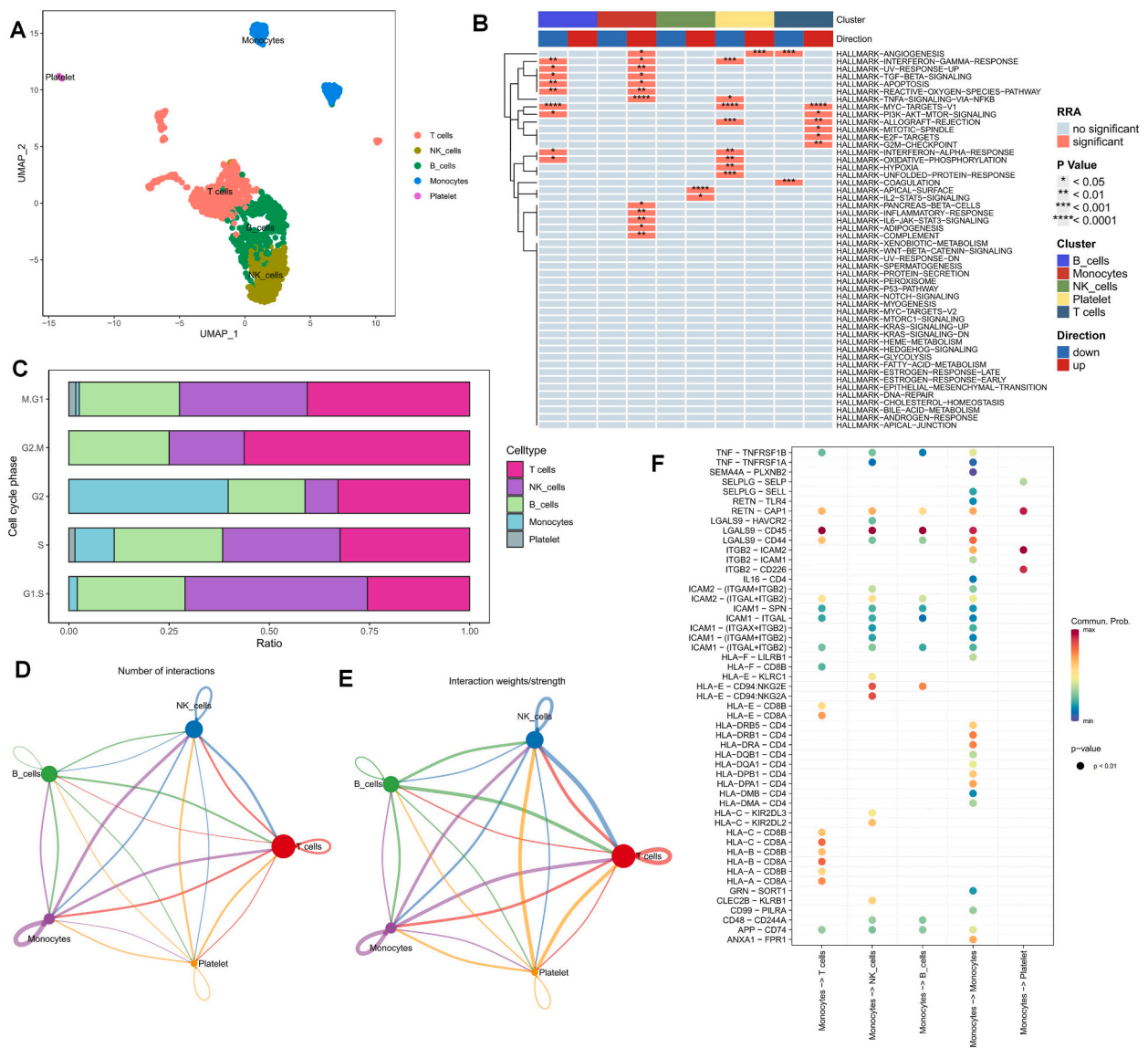


Fig. 3. Classification and analysis of cell subpopulations in peripheral blood of patients with Alzheimer's disease. (A) U-MAP plots of different cell subpopulations by color association. (B) GSEA plots showing the terms of the hallmark gene set enrichment pathway for each identified cell subpopulation. (C) The number of each cell subpopulation in proportion to the number of different cycles of cell development. (D,E) Number and strength of intercellular communication networks inferred by calculating the likelihood of communication, with the thickness of the lines representing strength or number. (F) Cellular signals from different cell types to monocytes. The vertical axis shows the interactions between receptors and ligands in selected cell types, with different colors representing the intensity. (For interpretation of the references to color in this figure legend, the reader is referred to the Web version of this article.)

to be mainly enriched in the disease group (Fig. 4A and B). Interestingly, in the peripheral blood cohort of AD, we observed a higher enrichment of monocyte-associated pathways in the normal group, while in the brain tissue cohort, they were enriched in the disease group (Fig. 4C and D). This suggests that monocytes in peripheral blood may have different biological effects in the progression of these two diseases. Additionally, we speculate that monocytes play a role in halting disease progression after entering brain and ovarian tissues through blood circulation. Subsequently, we conducted a differential analysis of monocyte-associated genes in OC peripheral blood using the “limma” package and identified 282 DEGs (Fig. 4E; Supplementary Table 1). Similarly, in the peripheral blood bulk sequencing data of AD, we identified 437 DEGs (Fig. 4F; Supplementary Table 2). Taking the intersection of these two sets of differential genes, we obtained 134 DEMRGs (Fig. 4G, Supplementary Table 3). The results of GO and KEGG enrichment analysis revealed that these genes were mainly associated with cell differentiation and chemokine-related pathways (Fig. 4H and I), and the results of DO enrichment analysis demonstrated their association with lung diseases, hematopoietic disorders, and leukemia (Fig. 4J).

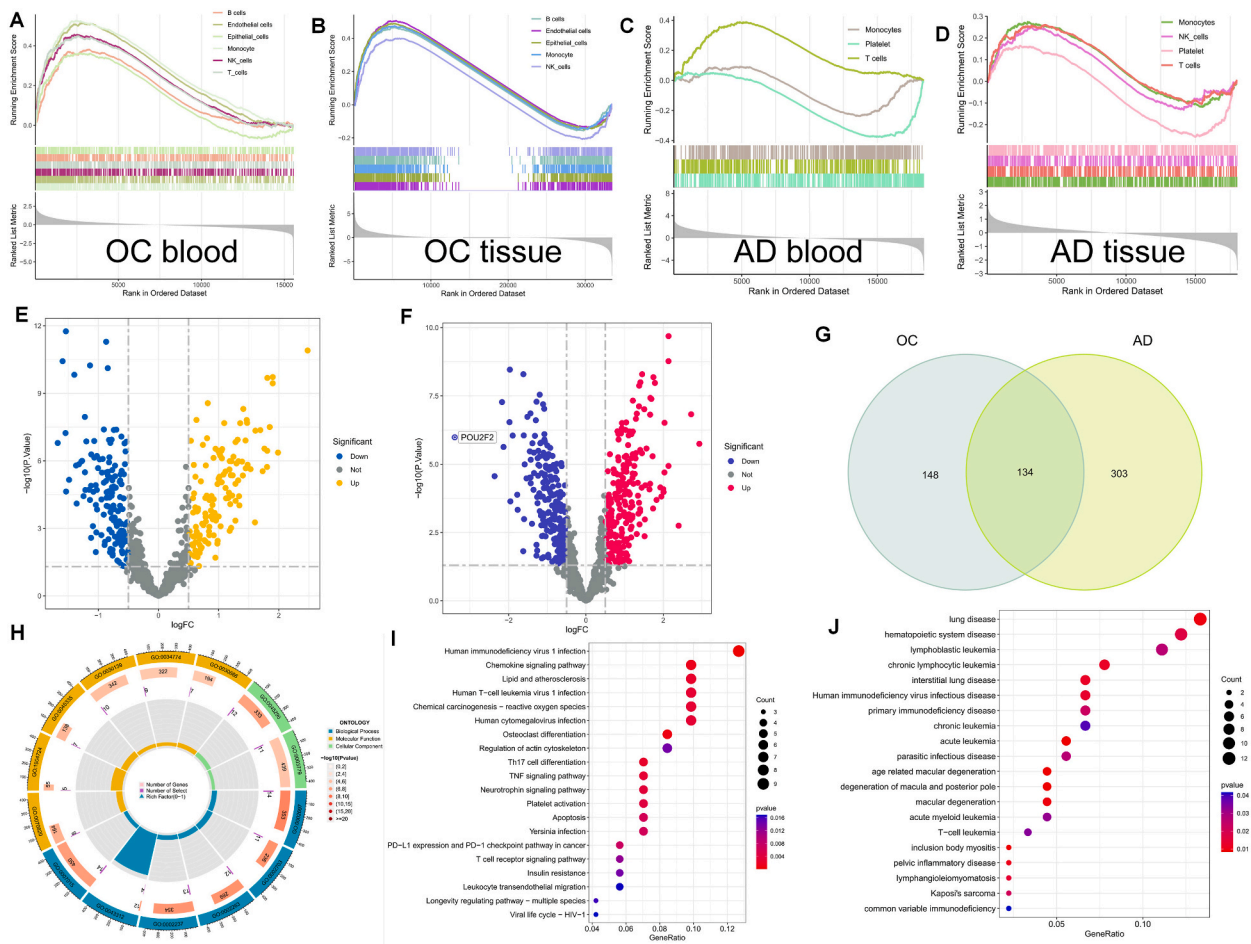


Fig. 4. Enrichment analysis of monocyte marker genes in ovarian cancer and Alzheimer's disease. (A–D) GSEA of 4 sets of peripheral blood and tissues for OC and AD, respectively. (E, F) Volcano plots showing differentially expressed MRGs in OC and AD peripheral blood cohorts. (G) Venn diagram showing DEMRGs co-expressed in OC and AD. (H, I, J) GO, KEGG and DO enrichment analysis of DEMRGs. MRGs, monocyte-related genes; DEMRGs, Differentially expressed monocyte-related genes; OC, Ovarian cancer; AD, Alzheimer's disease; GO, Gene Ontology; KEGG, Kyoto Encyclopedia of Genes and Genomes; DO, disease ontology.

3.5. Establishment of the monocyte-related prognostic signature in ovarian cancer

To quantify the risk for each ovarian cancer patient, a risk model based on monocyte-associated genes was constructed. Firstly, possible prognostic factors for OC patients were identified through univariate Cox analysis, resulting in 13 genes out of the 134 MRGs (Fig. 5A). Subsequently, a multivariate Cox regression analysis was performed to construct a precise risk model (Supplementary Table 4). The multivariate Cox regression analysis was conducted for the 13 prognosis-related genes, and a set of 7 genes was obtained for building the risk model, namely CFP, GAS7, ZFP36L1, UBE2R2, APOBEC3C, CUX1, and AP1S2. The risk score for each patient was calculated using the following equation: Risk score = $(-0.21 \times \text{CFP expression}) + (0.23 \times \text{GAS7 expression}) + (0.78 \times \text{ZFP36L1 expression}) + (-0.35 \times \text{UBE2R2 expression}) + (-0.36 \times \text{APOBEC3C expression}) + (0.40 \times \text{CUX1 expression}) + (-0.31 \times \text{AP1S2 expression})$. Considering the limited sample size of the GSE63885 cohort, the GSE9891 cohort and the GSE63885 cohort were merged to create a GEO validation cohort. Based on the median value of the risk score in the TCGA training cohort, patients were divided into high-risk (HR) and low-risk (LR) groups. Importantly, the LR group in the TCGA cohort exhibited a higher overall survival (OS) rate compared to the HR group (Fig. 5B). Similarly, in the GEO validation cohort, patients in the LR group demonstrated better OS (Fig. 5C). Moreover, patients in the HR group of the TCGA cohort showed worse progression-free survival (PFS) than those in the LR group (Fig. 5D). Furthermore, the monocyte-related risk model exhibited favorable performance in predicting OS for patients in the third and fifth years, with an AUC of 0.7 in the seventh year for both cohorts (Fig. 5E and F). The C-index of the risk score surpassed that of other clinical characteristics in both the TCGA and GEO cohorts (Fig. 5G and H).

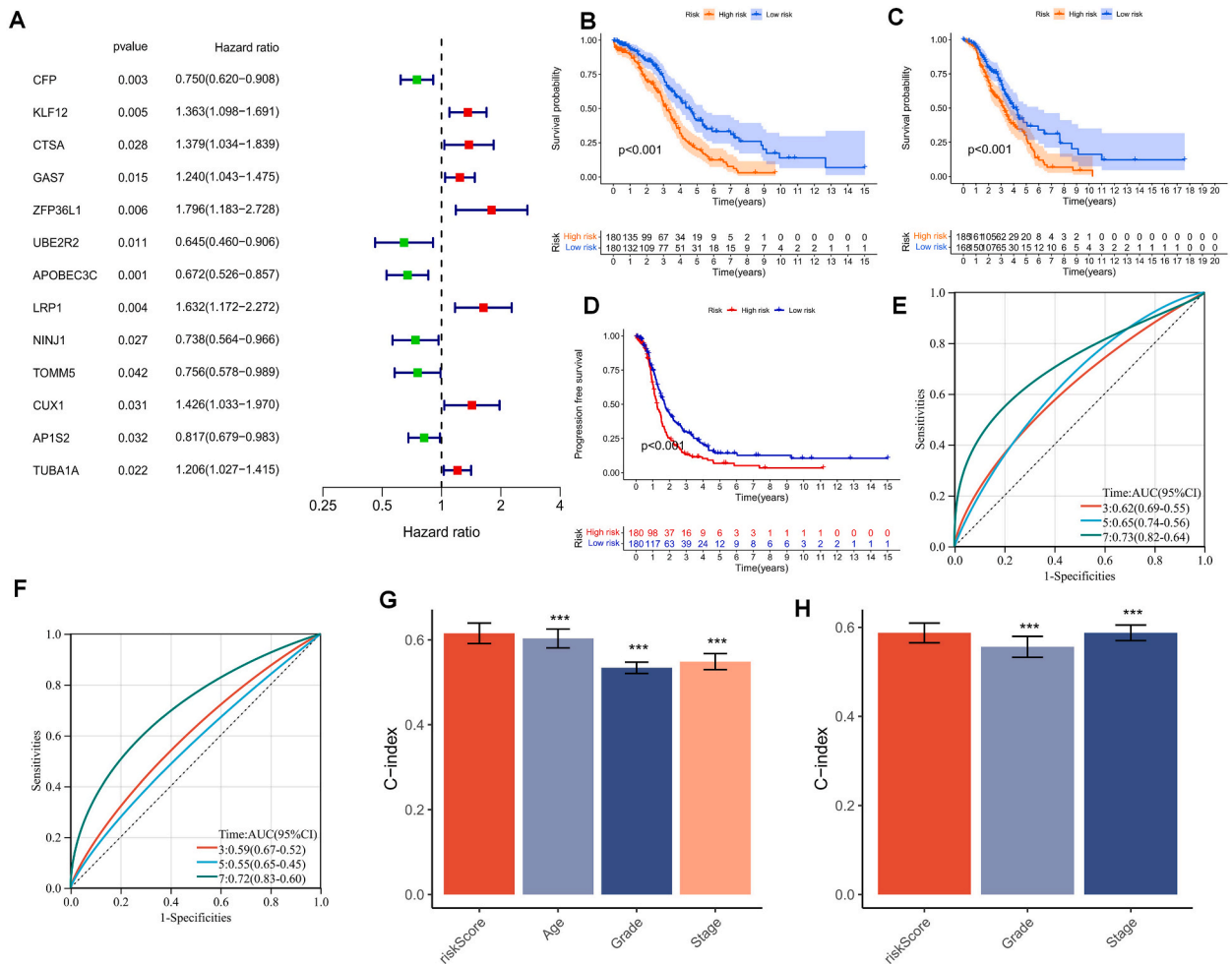


Fig. 5. Construction of monocyte-associated risk models and prognostic value of risk scores. (A) Forest plots showing the prognosis-related 13 MRGs screened with the univariate cox method. (B,C) Kaplan-Meier survival curves showing the risk stratification ability of the TCGA-OV and GEO cohorts. (D) Progression-free survival curves for the TCGA cohort. (E, F) AUC values of risk scores at 3, 5, and 7 years for the TCGA-OV and GEO cohorts. (G, H) Coherence index (C-index) of TCGA-OV and GEO cohorts. OC, Ovarian cancer; AD, Alzheimer’s disease, ***P < 0.001.

3.6. Validation of the prognostic signature associated with monocytes and construction of the nomogram

The risk score, determined through univariate and multivariate Cox analysis (Fig. 6A and B), was found to be an independent prognostic indicator for patients in the TCGA training set when compared to other common clinical characteristics such as age, grade, and stage. The validity of the risk model we developed was further confirmed in the GEO cohort (Fig. 6C and D). By assessing the correlation between the mentioned clinicopathological characteristics and the risk score, we developed a nomogram that could predict the 3-, 5-, and 7-year survival of OC patients (Fig. 6E). The accuracy of the nomogram prediction was demonstrated through calibration curves (Fig. 6F). Analysis depicted in Fig. 6G indicated that patients at stage IV exhibited higher risk scores, while patients with G3+G4 had risk scores similar to those with G1+G2 (Fig. 6H). These results provide robust evidence supporting the reliability of the monocyte-related prognostic model as a valuable clinical prediction tool.

3.7. TMB analysis and survival analysis of TMB

Genetic mutations are widely recognized as crucial factors in tumorigenesis. In our analysis using the TCGA database, we visually represented and correlated somatic mutation data with the constructed prognostic model. The top three mutated genes in both high and low-risk groups were TP53, TTN, and CSMD3 (Supplementary Figs. 3A–B). Furthermore, evidence suggests that patients with a high tumor mutational burden (TMB) may benefit from immunotherapy due to a higher number of antigens [43]. TMB analysis demonstrated a significant difference between the two groups, with the LR group exhibiting a higher TMB (Supplementary Fig. 3C). Kaplan-Meier survival analysis based on median TMB values, categorized into high and low TMB groups, further revealed a more favorable prognosis in the high TMB group, indicating that TMB could serve as an indicator of poor prognosis in OC patients

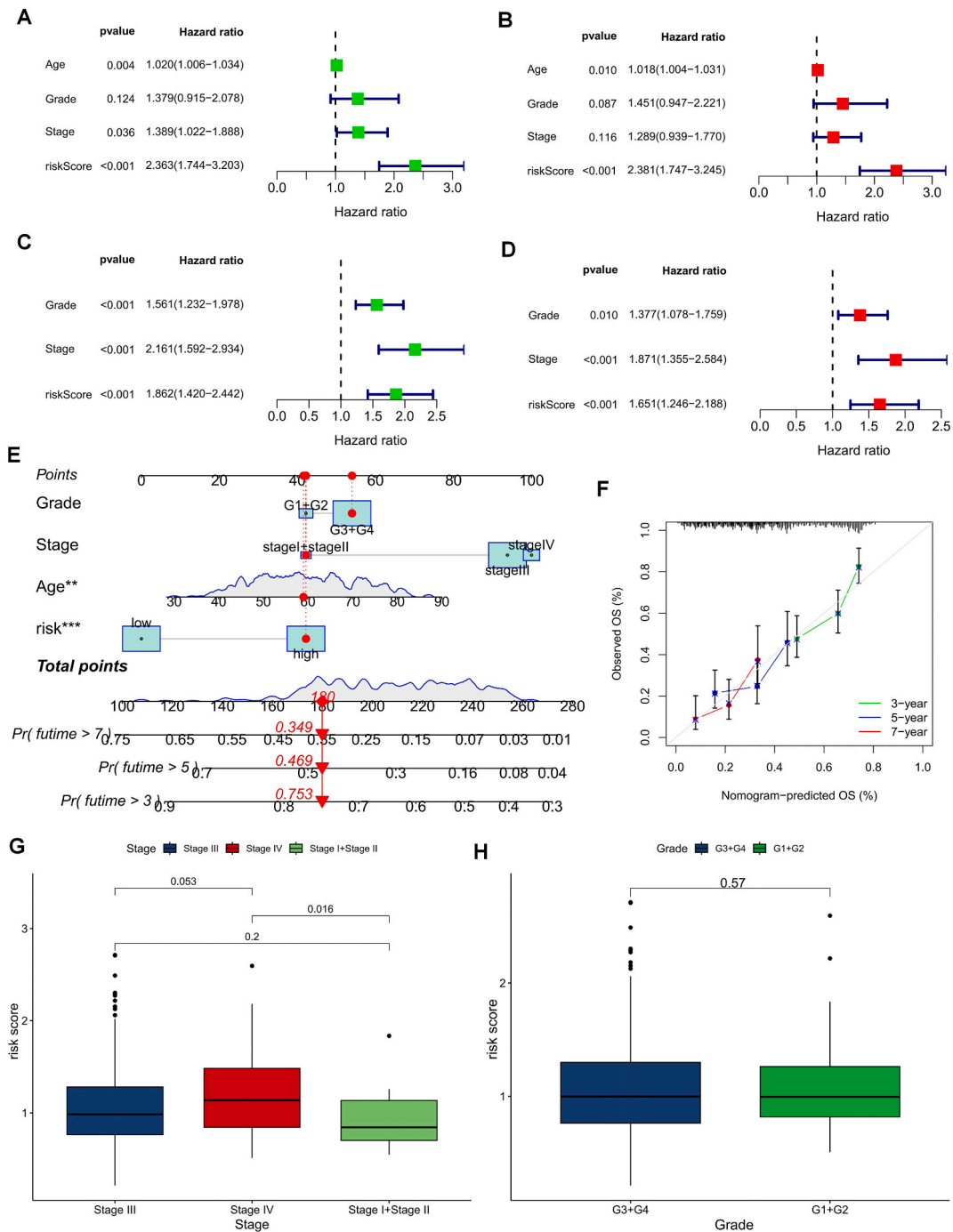


Fig. 6. Independent prognostic analysis and construction of nomograms for risk scores of ovarian cancer patients. Univariate and multivariate Cox regression analysis of clinicopathological variables and OS risk scores for the TCGA training cohort (A, B) and GEO validation cohort (C, D). (E, F) Nomograms and calibration curves for predicting OS at 3, 5 and 7 years in patients with OC. (G,H) Risk scores for patients with different stage and grade. *P < 0.05; **P < 0.01; ***P < 0.001.

(Supplementary Fig. 3D). By combining the risk score and TMB, patients were divided into four subgroups for survival assessment. The high TMB and low-risk groups exhibited the best prognosis, validating the model and identifying the most favorable prognostic subgroup for clinical application (Supplementary Fig. 3E).

In addition, we employed the IMvigor 210 cohort, which comprises patients receiving *anti*-PD-L1 immunotherapies, to evaluate the predictive value of our risk score in determining the response to immunotherapy. Among the 298 samples, we divided them into two groups based on the median risk scores calculated using the previously mentioned formula. We observed significant differences in risk scores between the groups showing remission (Fig. 8A), with a higher proportion of complete or partial responses (CR/PR) found in the lower risk group (Fig. 8B). To further refine the selection of patients who are more suitable for immunotherapy, we utilized the TIDE score to assess potential abnormalities in immune function within the tumor and regional lymph nodes. A higher TIDE prediction score indicates a higher likelihood of immune evasion, suggesting that patients are less likely to benefit from immune checkpoint inhibitor (ICI) treatment. According to the TIDE results, all patients in the lower risk (LR) group exhibited the potential for an effective immune response (Fig. 8C). The area under the ROC curve (AUC) reached 0.78, demonstrating the efficacy of the MRG risk score in predicting the response to immunotherapy (Fig. 8D). Furthermore, patients in the LR group had a higher probability of responding favorably to immunotherapy (Fig. 8E). These findings support the notion that patients in the LR group not only have a better prognosis but also demonstrate enhanced immune function, indicating their potential sensitivity to immunotherapy.

3.9. Selection of characteristic genes in Alzheimer's disease and ovarian cancer

In the brain cortical sequencing GSE5281 cohort, two algorithms were used to select genes associated with signature genes for AD

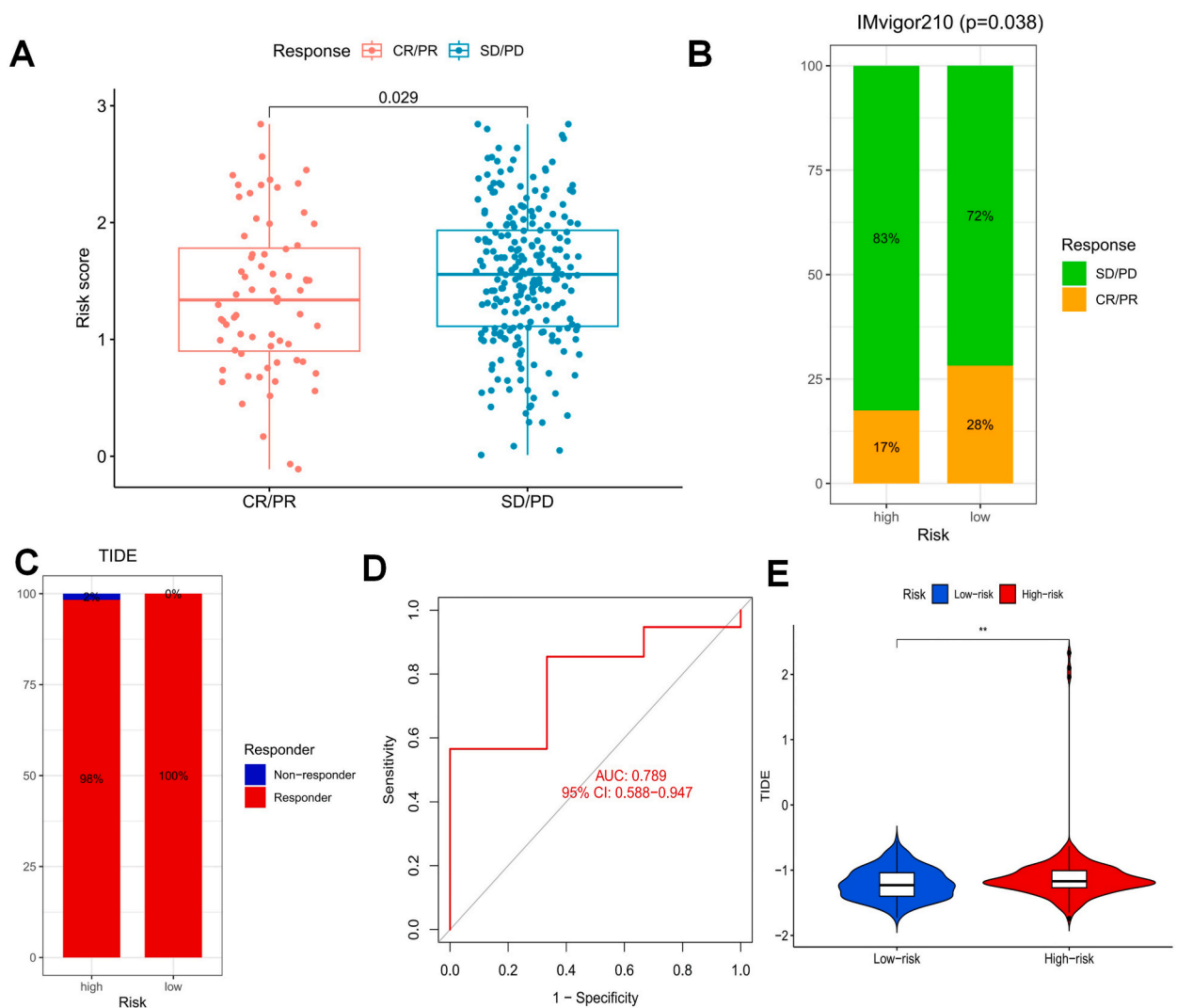


Fig. 8. Correlation of MRG-associated risk scores and immunotherapy effects. (A) Differences in risk scores between response groups in the IMvigor210 cohort. (B) Proportion of *anti*-PD-L1 immunotherapy responses in high-risk and low-risk populations. (C) Proportion of immunotherapy responses in high- and low-risk populations based on TIDE results. (D) Risk scores for predicting whether to generate an effective immunotherapy response by ROC curves. (E) Difference in TIDE scores between the high-risk and low-risk groups. CR, complete remission; PR, partial remission; SD, stable disease; PD, Progressive disease. * $p < 0.05$; ** $p < 0.01$; *** $p < 0.001$; MRGs, monocyte-related genes.

progression. According to the 134 intersecting genes obtained from Fig. 4G, for the SVM-RFE algorithm, the classifier had the lowest error rate when the number of features was 25 (Fig. 9A; Supplementary Table 5). The random forest algorithm screened 66 feature genes with relative importance)0 (Fig. 9B and C; Supplementary Table 6). By taking the intersection with the risk model genes of OC, we finally identified 2 feature genes, ZFP36L1 and AP1S2, which are common to OC signature, Random Forest and SVM-RFE algorithms (Fig. 9D). We also evaluated the diagnostic performance of two signature genes in the TCGA-GTEX cohort and the GSE5281 cohort in predicting OC and AD progression. The AUC values of the ROC curves in the OC cohort were 0.804 for ZFP36L1 and 0.810 for AP1S2, respectively (Fig. 9E). The AUC values of the ROC curves in the AD cohort were 0.883 for ZFP36L1 and 0.882 for AP1S2, respectively (Fig. 9F). In addition in the peripheral blood single cell sequencing data of OC and AD, we found that both ZFP36L1 and AP1S2 were predominantly expressed in monocytes/macrophages (Fig. 9G and H).

3.10. Validation of signature gene expression in ovarian cancer cell lines

We further validated the expression patterns of ZFP36L1 and AP1S2 in ovarian cancer (OC) patients using immunohistochemical data from the Human Protein Atlas (HPA) database. Our analysis revealed that AP1S2 protein expression levels were significantly increased in ovarian cancer tissues compared to healthy ovarian tissues (Fig. 10A and B). Conversely, ZFP36L1 protein expression was significantly decreased in ovarian cancer (Fig. 10E and F). Moreover, quantitative real-time polymerase chain reaction (qRT-PCR) analysis demonstrated that AP1S2 expression levels were significantly up-regulated in ovarian cancer cell lines (Fig. 10C and D), whereas ZFP36L1 expression levels were relatively down-regulated (Fig. 10G and H). These findings suggest that the dysregulated expression of these genes may contribute to the oncogenic transformation of ovarian cancer.

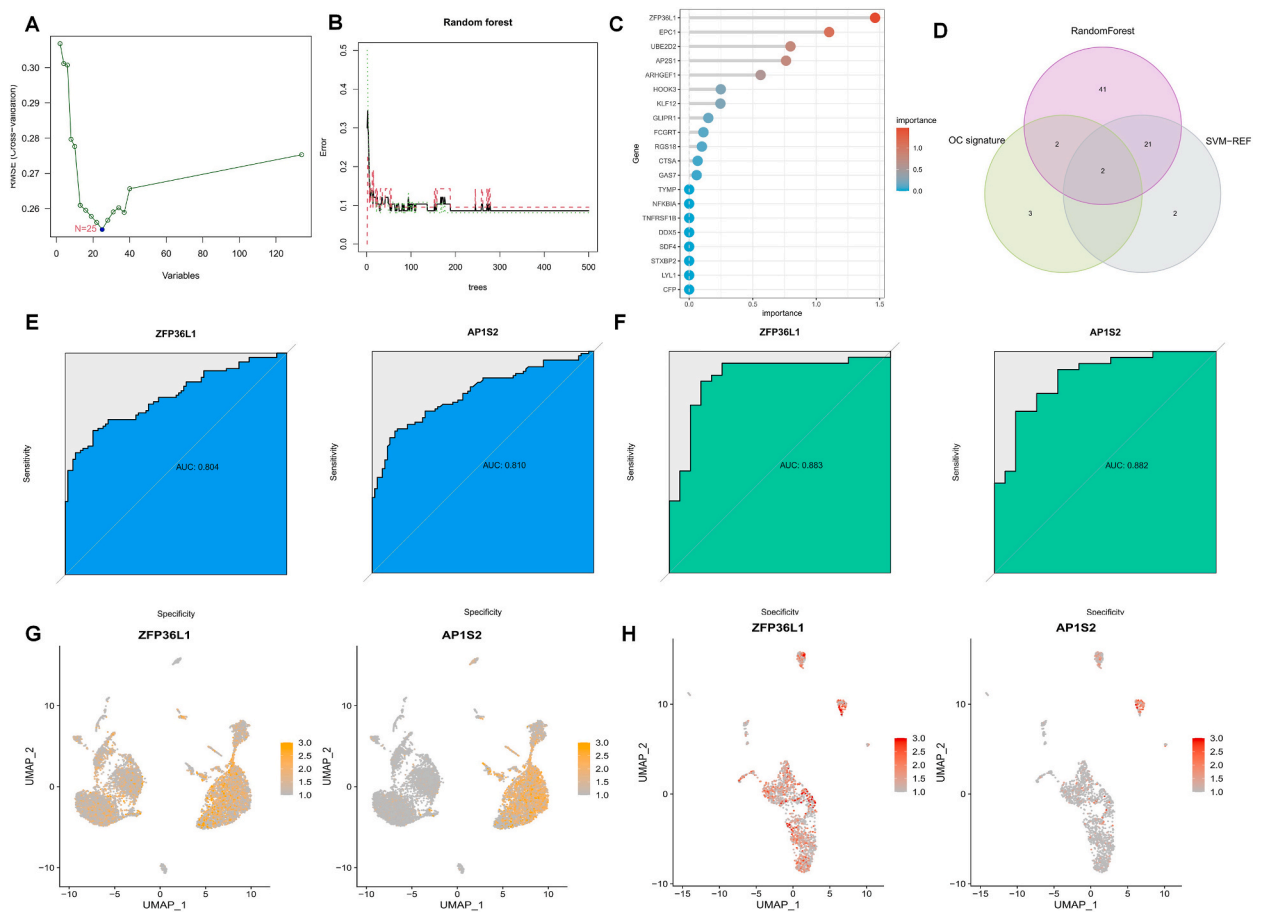


Fig. 9. Selection of signature genes and estimation of their diagnostic efficacy by means of machine learning. (A) SVM-RFE feature selection algorithm. (B) Error rate of random forest with the number of decision trees. (C) Gene order according to the relative importance of genes. (D) Venn diagram showing the intersection genes of OC risk model, random forest and SVM-RFE algorithm. (E,F) ROC curves for estimating the diagnostic performance of ZFP36L1 and AP1S2 in the GEO and TCGA-GTEX cohorts. (G,H) UMAP was used to demonstrate ZFP36L1 and AP1S2 expression in OC and AD at the peripheral blood single cell level. OC Ovarian cancer; AD, Alzheimer's disease.

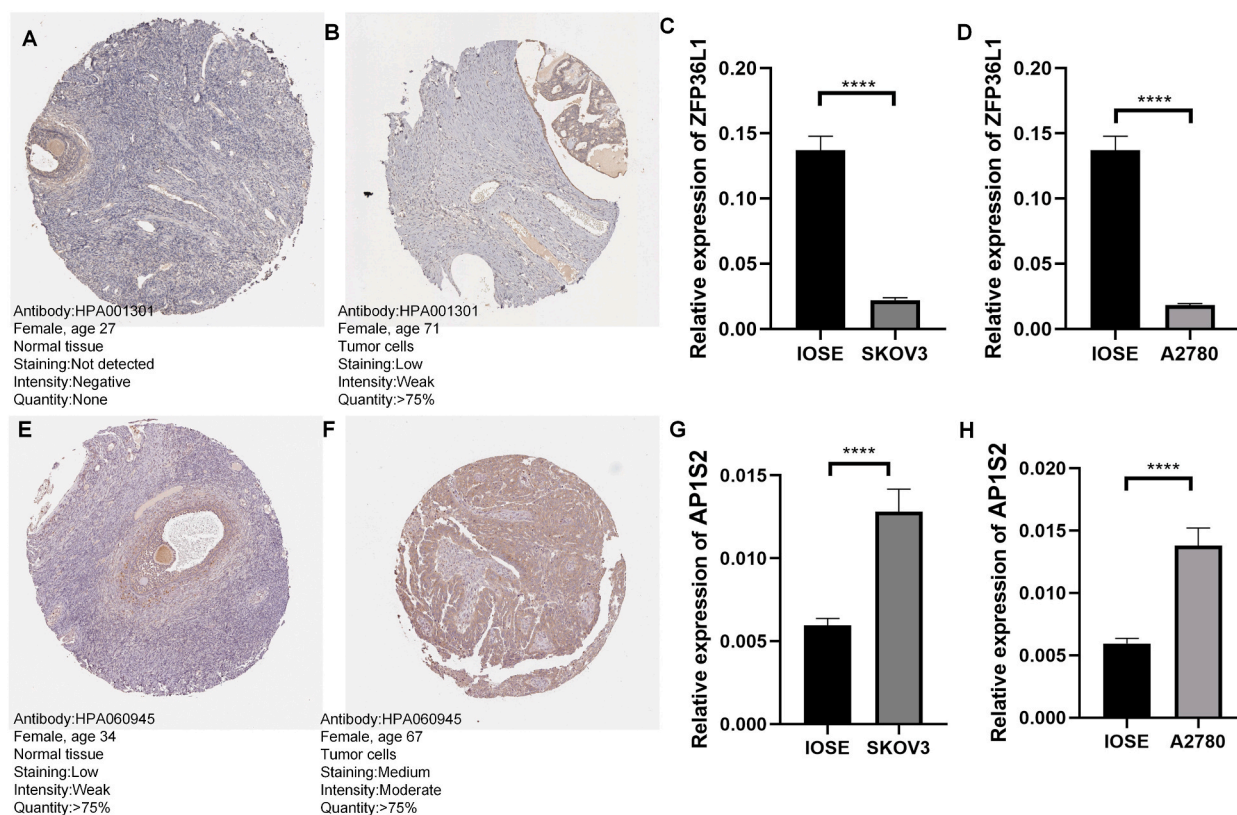


Fig. 10. Expression validation of MRGs that constitute a risk model in ovarian cancer cell lines. (A,B) Immunohistochemical analysis of ZFP36L1 in normal ovarian tissue and ovarian cancer. (C,D) qRT-PCR analysis of ZFP36L1 in normal ovarian epithelial cells and two tumor cells. (E, F) Immunohistochemical analysis of AP1S2 in normal ovarian tissues and ovarian carcinomas. (G,H) qRT-PCR analysis of AP1S2 in normal ovarian epithelial cells and two tumor cells. **** $p < 0.0001$.

4. Discussion

Although Alzheimer's and ovarian cancer are two different diseases, there are some connections between them. Patients with Alzheimer's may face several additional risk factors that increase the likelihood of developing ovarian cancer. These risk factors may be associated with the physical and behavioral changes caused by Alzheimer's, such as long-term use of certain medications, poor nutrition, and reduced physical activity. Additionally, patients with dementia may experience cognitive and behavioral impairments that could lead to neglecting their health, potentially affecting early detection and treatment of ovarian cancer. While a specific causal relationship is not yet clear, these associations highlight the importance of enhanced ovarian cancer risk assessment and preventive measures in patients with dementia. However, since both diseases are more prevalent in middle-aged and older populations, research suggests that factors like genetics, lifestyle, and chronic diseases are linked to an increased risk of Alzheimer's disease and ovarian cancer [45–48]. For example, epidemiological studies indicate that diabetes and hypertension may contribute to the development of Alzheimer's disease [49]. Similarly, a study conducted in the United States found associations between hypertension, hyperlipidemia, and an increased risk of ovarian cancer [50].

Another perspective is that, in contrast to the excessive neuronal cell death observed in Alzheimer's disease, cancer is characterized by unrestricted cell proliferation and a strong resistance to cell death [9]. According to some epidemiological studies, patients with dementia appear to have a lower risk of developing cancer. For instance, a recent study observed a lower risk of cancer, especially ovarian cancer, in individuals with Alzheimer's compared to those without Alzheimer's [51]. This observation may be related to the altered regulatory mechanisms of cell proliferation and cell death found in Alzheimer's patients [52]. However, it is important to note that the current understanding of the relationship between Alzheimer's and cancer is still limited, and contradictory findings exist. Further research is needed to delve into the potential link between Alzheimer's and cancer, considering the combined effects of genetic, environmental, and lifestyle factors [53]. Therefore, while some studies suggest that individuals with dementia may have a lower likelihood of developing cancer, more research is required to fully comprehend the relationship between the two diseases and the possible influence of biological and environmental factors on their interactions.

Monocytes, which possess phagocytic and antigen presentation capabilities, are often considered immature macrophages, leading some researchers to group them within the monocyte/macrophage category. Studies have observed that Alzheimer's patients exhibit elevated numbers and increased activation status of monocytes in their bloodstream. This monocyte activation can trigger

neuroinflammatory responses characterized by the release of inflammatory mediators and cytokines, resulting in neuronal apoptosis, synaptic damage, and glial inflammation [54,55]. Furthermore, research suggests that vascular inflammation, impairment of the blood-brain barrier, and immune response imbalances can activate monocytes, thereby exacerbating neuroinflammatory responses and promoting the onset and progression of Alzheimer's disease [56,57]. However, some studies propose that monocytes may also play a protective role in Alzheimer's disease by secreting neurotrophic and anti-inflammatory factors that facilitate neuronal development, repair, and neuroprotection [58,59].

Numerous studies have extensively documented the elevated levels and activated state of monocytes in the peripheral blood of patients with ovarian cancer. These monocytes have been implicated in the development and progression of tumors by promoting tumor cell proliferation, invasion, and metastasis [60]. Through the secretion of growth factors, chemokines, and inflammatory mediators, monocytes have the capacity to activate various cell types in the tumor microenvironment, including tumor-associated macrophages (TAMs) and T cells. This process contributes to the establishment of a malignant microenvironment that supports tumor growth and metastasis [61]. Furthermore, the expression of PD-L1 on ascites and blood monocytes in ovarian cancer patients has been associated with unfavorable clinical outcomes [62].

To fully comprehend the involvement of monocytes in the pathogenesis of Alzheimer's disease and ovarian cancer, additional research is warranted for validation and establishing their precise roles. However, investigating the link between these two diseases holds significant significance, as it can provide valuable insights for the development of preventive and therapeutic strategies. In our study, we employed single-cell RNA sequencing (scRNA-seq) of peripheral blood to investigate the potential biological and immune-related functions of monocytes/macrophages in these diseases. Our findings emphasized the critical role of Human Leukocyte Antigen (HLA) molecules in the immune system's functioning in both conditions. Notably, the expression level of HLA-DR molecules on the surface of monocytes can serve as an indicator of their activation status and function, which can influence the occurrence and progression of various diseases [63]. In the context of ovarian cancer, HLA signaling is implicated in immune evasion, immune activation, and immune regulation. Reduced HLA expression or deficiency has been associated with unfavorable prognosis in ovarian cancer patients [64]. Through differential analysis, we identified a set of 134 monocyte-related genes (MRGs) and developed a unique prognostic signature for ovarian cancer patients in the TCGA database. We validated the predictive potential of this signature in an external GEO cohort, and the AUC values of the ROC curve demonstrated its predictive power. Furthermore, our risk score correlated with the patient's clinical stage, and clinical variables with high-risk scores were significant prognostic factors, indicating that the monocyte-associated gene signature could serve as a prognostic predictor in ovarian cancer.

In ovarian cancer, mutations in genes associated with a high tumor mutational burden (TMB) primarily involve DNA repair-related genes such as BRCA1 and BRCA2, tumor suppressor genes like TP53, and other genes including NF1 and RB1, which potentially contribute to ovarian cancer development and progression [65]. Research on ovarian cancer patients has demonstrated that those with high TMB levels exhibit longer overall and progression-free survival rates after immunotherapy, indicating that TMB could serve as a significant predictor of immunotherapy response in ovarian cancer patients [66]. Our study suggests that patients in the low-risk group display relatively higher TMB levels, indicating their potential suitability for immunotherapy. The expression level of PD-L1 in ovarian cancer patients' tumor tissues is closely associated with patient prognosis. Consequently, we further investigated the immune microenvironment and conducted an expression analysis of immune checkpoint genes in different risk subgroups. Our study revealed that patients in the low-risk group exhibited greater immune cell infiltration, enrichment of immune-related functions, and higher expression of immune checkpoints. These findings likely contribute to the distinct prognosis and response rates to immunotherapy observed between the two groups. Tumor Immune Dysfunction and Exclusion (TIDE) is a recently identified predictor of immunotherapy response that outperforms other biomarkers or clinical features [67]. To enhance the reliability of our conclusions, we included a real cohort of bladder cancer patients who underwent immunotherapy in the IMvigor 210 trial. Collectively, these results suggest that the low-risk group experiences greater benefits from immunotherapy compared to the high-risk group.

In our study, we identified ZFP36L1 and AP1S2 as constituting a stable risk score signature for ovarian cancer and also being signature genes for Alzheimer's disease (AD). ZFP36L1 is involved in the post-transcriptional regulation of gene expression and has been shown to impact cancer cells functionally. Silencing ZFP36L1 enhances tumor cell growth, while its overexpression inhibits cell proliferation and migration in bladder and breast cancer cell lines. One mechanism through which ZFP36L1 inhibits cell proliferation is by down-regulating the expression of the cell cycle protein D, leading to cell cycle arrest in the G1 phase [68,69]. ZFP36L1 has also been identified as one of the variant genes associated with an increased risk of epithelial ovarian cancer [70]. However, there is limited research on the role of ZFP36L1 in AD. Some bioinformatic studies suggest that the zinc finger protein ZFP36L1 is a target of multiple microRNAs in Alzheimer's disease [71]. AP1S2 has been reported as a prognostic marker in ovarian cancer, and its expression levels differ in drug-resistant cell lines [72]. In melanoma, downregulation of AP1S2 inhibits tumor cell migration, indicating its potential as a therapeutic target [73]. However, there are no studies on AP1S2 in neurodegenerative diseases, although mutations in AP1S2 have been noted in cases of fourth ventricular foramen occlusion syndrome with intellectual disability, basal ganglia disease, and seizures [74].

To further advance our understanding of the roles of monocytes in ovarian cancer and Alzheimer's disease, future research can be focused on the following perspectives. Firstly, the molecular mechanisms by which monocytes contribute to disease onset and development need to be explored, including their functions and regulatory pathways. Secondly, the interactions between monocytes, tumor cells, and immune cells, as well as their impact on tumor immune evasion, should be investigated. Finally, the effects of monocytes on neurons through the release of inflammatory factors and oxidative stress substances need to be examined to explore the potential of monocytes in the treatment of neurodegenerative diseases. Further research in these areas can deepen our understanding of the relationship between monocytes and these diseases, providing important theoretical support for the development of new therapeutic strategies.

While our prognostic signature comprising monocyte-associated genes has shown promising results in identifying immune signatures and predicting patient prognosis, there are several limitations that should be addressed in future studies [75,76]. Firstly, differences in sequencing platforms can introduce variations in sequencing errors, which can be biological, random, or systematic, such as batch effects. Future studies will require more advanced techniques and tools for data analysis to uncover genuine biological differences between samples and develop robust model-building methods. Additionally, analysis based on public databases may introduce biases in prediction results, necessitating validation using real data from ovarian cancer patients. Moreover, the biological roles and mechanisms of the two monocyte-associated genes, ZFP36L1 and AP1S2, in both diseases warrant further investigation.

Author contribution statement

Songyun Zhao; Jinhui Liu: Conceived and designed the experiments. Jinhui Liu: Performed the experiments. Songyun Zhao; Bicheng Ye: Analyzed and interpreted the data. Hao Chi; Chao Cheng: Contributed reagents, materials, analysis tools or data. Songyun Zhao; Jinhui Liu; Chao Cheng: Wrote the paper.

Funding statement

This work was supported by Wuxi Taihu Lake Talent Plan, Supports for Leading Talents in Medical and Health Profession (2020THRC-DJ-SNW) and the Jiangsu Province Nature Science Foundation (BK20220729).

Data availability statement

The datasets analyzed for this study were obtained from the UCSC Xena website (<https://xenabrowser.net/datapages/>) and GEO dataset (<https://www.ncbi.nlm.nih.gov/geo/>).

Ethics statement

This article does not contain any studies with human participants or animals.

Declaration of competing interest

The authors declare no conflicts of interest.

Acknowledgment

We thank all the participants involved in this study.

Appendix A. Supplementary data

Supplementary data to this article can be found online at <https://doi.org/10.1016/j.heliyon.2023.e17454>.

References

- [1] M. Meryet-Figuere, et al., Atelocollagen-mediated in vivo siRNA transfection in ovarian carcinoma is influenced by tumor site, siRNA target and administration route, *Oncol. Rep.* 38 (4) (2017) 1949–1958.
- [2] R. Geng, et al., The m6A-related long noncoding RNA signature predicts prognosis and indicates tumor immune infiltration in ovarian cancer, *Cancers* 14 (16) (2022).
- [3] B.H. Koehn, S.P. Schoenberger, Tumor immunotherapy: making an immortal army, *Nat. Med.* 15 (7) (2009) 731–732.
- [4] R.L. Coleman, et al., Latest research and treatment of advanced-stage epithelial ovarian cancer, *Nat. Rev. Clin. Oncol.* 10 (4) (2013) 211–224.
- [5] R.G. Tremblay, et al., Differentiation of mouse Neuro 2A cells into dopamine neurons, *J. Neurosci. Methods* 186 (1) (2010) 60–67.
- [6] W.Y. Fu, X. Wang, N.Y. Ip, Targeting neuroinflammation as a therapeutic strategy for Alzheimer's disease: mechanisms, drug candidates, and new opportunities, *ACS Chem. Neurosci.* 10 (2) (2019) 872–879.
- [7] H. Hampel, et al., Alzheimer's disease biomarker-guided diagnostic workflow using the added value of six combined cerebrospinal fluid candidates: abeta(1-42), total-tau, phosphorylated-tau, NFL, neurogranin, and YKL-40, *Alzheimers Dement* 14 (4) (2018) 492–501.
- [8] K.B. Rajan, et al., Population estimate of people with clinical Alzheimer's disease and mild cognitive impairment in the United States (2020-2060), *Alzheimers Dement* 17 (12) (2021) 1966–1975.
- [9] P.S. Filippou, T.F. Outeiro, Cancer and Parkinson's disease: common targets, emerging hopes, *Mov. Disord.* 36 (2) (2021) 340–346.
- [10] H. Plun-Favreau, et al., Cancer and neurodegeneration: between the devil and the deep blue sea, *PLoS Genet.* 6 (12) (2010), e1001257.
- [11] S.D. Karanth, et al., Cancer diagnosis is associated with a lower burden of dementia and less Alzheimer's-type neuropathology, *Brain* 145 (7) (2022) 2518–2527.
- [12] C. Lanni, et al., Cancer and Alzheimer's disease inverse relationship: an age-associated diverging derailment of shared pathways, *Mol. Psychiatr.* 26 (1) (2021) 280–295.
- [13] Y. Yan, et al., X-linked ubiquitin-specific peptidase 11 increases tauopathy vulnerability in women, *Cell* 185 (21) (2022) 3913–3930 e19.
- [14] E.C. Evans, et al., Salpingo-oophorectomy at the time of benign hysterectomy: a systematic review, *Obstet. Gynecol.* 128 (3) (2016) 476–485.
- [15] C.S. Ulbjerg, et al., Oophorectomy and rate of dementia: a prospective cohort study, *Menopause* 29 (5) (2022) 514–522.

- [16] A. Bagit, G.C. Hayward, R.E.K. MacPherson, Exercise and estrogen: common pathways in Alzheimer's disease pathology, *Am. J. Physiol. Endocrinol. Metab.* 321 (1) (2021) E164–E168.
- [17] M.S. Uddin, et al., Estrogen signaling in Alzheimer's disease: molecular insights and therapeutic targets for Alzheimer's dementia, *Mol. Neurobiol.* 57 (6) (2020) 2654–2670.
- [18] X.N. Shen, et al., Inflammatory markers in Alzheimer's disease and mild cognitive impairment: a meta-analysis and systematic review of 170 studies, *J. Neurol. Neurosurg. Psychiatry* 90 (5) (2019) 590–598.
- [19] S. Guleria, et al., Risk of epithelial ovarian cancer among women with benign ovarian tumors: a follow-up study, *Cancer Causes Control* 31 (1) (2020) 25–31.
- [20] S. Zhao, et al., Identification of copper metabolism-related subtypes and establishment of the prognostic model in ovarian cancer, *Front. Endocrinol.* 14 (2023), 1145797.
- [21] A. Conesa, et al., A survey of best practices for RNA-seq data analysis, *Genome Biol.* 17 (2016) 13.
- [22] Y. Ren, et al., Single-cell sequencing reveals effects of chemotherapy on the immune landscape and TCR/BCR clonal expansion in a relapsed ovarian cancer patient, *Front. Immunol.* 13 (2022), 985187.
- [23] D. Pils, et al., A combined blood based gene expression and plasma protein abundance signature for diagnosis of epithelial ovarian cancer—a study of the OVCAD consortium, *BMC Cancer* 13 (2013) 178.
- [24] H. Xu, J. Jia, Single-cell RNA sequencing of peripheral blood reveals immune cell signatures in Alzheimer's disease, *Front. Immunol.* 12 (2021), 645666.
- [25] B.J. Naughton, et al., Blood genome-wide transcriptional profiles reflect broad molecular impairments and strong blood-brain links in Alzheimer's disease, *J. Alzheimers Dis* 43 (1) (2015) 93–108.
- [26] W.S. Liang, et al., Gene expression profiles in anatomically and functionally distinct regions of the normal aged human brain, *Physiol. Genom.* 28 (3) (2007) 311–322.
- [27] R.A. Irizarry, et al., Exploration, normalization, and summaries of high density oligonucleotide array probe level data, *Biostatistics* 4 (2) (2003) 249–264.
- [28] D. Aran, et al., Reference-based analysis of lung single-cell sequencing reveals a transitional profibrotic macrophage, *Nat. Immunol.* 20 (2) (2019) 163–172.
- [29] P. Zhang, et al., The integrated single-cell analysis developed a lactate metabolism-driven signature to improve outcomes and immunotherapy in lung adenocarcinoma, *Front. Endocrinol.* 14 (2023), 1154410.
- [30] I. Korsunsky, et al., Fast, sensitive and accurate integration of single-cell data with Harmony, *Nat. Methods* 16 (12) (2019) 1289–1296.
- [31] D. Sinha, et al., dropClust: efficient clustering of ultra-large scRNA-seq data, *Nucleic Acids Res.* 46 (6) (2018) e36.
- [32] S.C. Zheng, et al., Universal prediction of cell-cycle position using transfer learning, *Genome Biol.* 23 (1) (2022) 41.
- [33] S. Jin, et al., Inference and analysis of cell-cell communication using CellChat, *Nat. Commun.* 12 (1) (2021) 1088.
- [34] S. Zhao, et al., Crosstalk of disulfidoptosis-related subtypes, establishment of a prognostic signature and immune infiltration characteristics in bladder cancer based on a machine learning survival framework, *Front. Endocrinol.* 14 (2023), 1180404.
- [35] G. Yu, et al., clusterProfiler: an R package for comparing biological themes among gene clusters, *OMICS* 16 (5) (2012) 284–287.
- [36] S. Hanzelmann, R. Castelo, J. Guinney, GSEA: gene set variation analysis for microarray and RNA-seq data, *BMC Bioinf.* 14 (2013) 7.
- [37] P. Zhang, et al., By integrating single-cell RNA-seq and bulk RNA-seq in sphingolipid metabolism, CACYBP was identified as a potential therapeutic target in lung adenocarcinoma, *Front. Immunol.* 14 (2023), 1115272.
- [38] S. Mariathasan, et al., TGFbeta attenuates tumour response to PD-L1 blockade by contributing to exclusion of T cells, *Nature* 554 (7693) (2018) 544–548.
- [39] J. Xie, et al., The pan-cancer multi-omics landscape of FOXO family relevant to clinical outcome and drug resistance, *Int. J. Mol. Sci.* 23 (24) (2022).
- [40] A. Mayakonda, et al., Maftools: efficient and comprehensive analysis of somatic variants in cancer, *Genome Res.* 28 (11) (2018) 1747–1756.
- [41] S. Zhao, et al., Machine learning-based characterization of cuproptosis-related biomarkers and immune infiltration in Parkinson's disease, *Front. Genet.* 13 (2022), 1010361.
- [42] H. Sanz, et al., SVM-RFE: selection and visualization of the most relevant features through non-linear kernels, *BMC Bioinf.* 19 (1) (2018) 432.
- [43] T.A. Chan, et al., Development of tumor mutation burden as an immunotherapy biomarker: utility for the oncology clinic, *Ann. Oncol.* 30 (1) (2019) 44–56.
- [44] S. Zhao, et al., Expression of hub genes of endothelial cells in glioblastoma-A prognostic model for GBM patients integrating single-cell RNA sequencing and bulk RNA sequencing, *BMC Cancer* 22 (1) (2022) 1274.
- [45] A. Martowicz, A. Seeber, G. Untergasser, The role of EpCAM in physiology and pathology of the epithelium, *Histol. Histopathol.* 31 (4) (2016) 349–355.
- [46] Y.S. Seo, et al., Dietary carbohydrate constituents related to gut dysbiosis and health, *Microorganisms* 8 (3) (2020).
- [47] D. Samuel, et al., Hereditary ovarian carcinoma: cancer pathogenesis looking beyond BRCA1 and BRCA2, *Cells* 11 (3) (2022).
- [48] H. Zhao, et al., Inflammation and tumor progression: signaling pathways and targeted intervention, *Signal Transduct. Targeted Ther.* 6 (1) (2021) 263.
- [49] P.K. Kamat, et al., Homocysteine, alcoholism, and its potential epigenetic mechanism, *Alcohol Clin. Exp. Res.* 40 (12) (2016) 2474–2481.
- [50] K.A. Michels, T.S. McNeel, B. Trabert, Metabolic syndrome and risk of ovarian and fallopian tube cancer in the United States: an analysis of linked SEER-Medicare data, *Gynecol. Oncol.* 155 (2) (2019) 294–300.
- [51] A.Z. Sherzai, et al., Alzheimer disease and cancer: a national inpatient sample analysis, *Alzheimer Dis. Assoc. Disord.* 34 (2) (2020) 122–127.
- [52] X. Li, et al., OCIAD1 contributes to neurodegeneration in Alzheimer's disease by inducing mitochondria dysfunction, neuronal vulnerability and synaptic damages, *EBioMedicine* 51 (2020), 102569.
- [53] S. Zhao, et al., Identification and validation of neurotrophic factor-related gene signatures in glioblastoma and Parkinson's disease, *Front. Immunol.* 14 (2023), 1090040.
- [54] R.S. Doody, et al., A phase 3 trial of semagacestat for treatment of Alzheimer's disease, *N. Engl. J. Med.* 369 (4) (2013) 341–350.
- [55] N. Sladojevic, et al., Inhibition of junctional adhesion molecule-A/LFA interaction attenuates leukocyte trafficking and inflammation in brain ischemia/reperfusion injury, *Neurobiol. Dis.* 67 (2014) 57–70.
- [56] M.L. Block, L. Calderon-Garciduenas, Air pollution: mechanisms of neuroinflammation and CNS disease, *Trends Neurosci.* 32 (9) (2009) 506–516.
- [57] L. Vanherle, et al., Improving cerebrovascular function to increase neuronal recovery in neurodegeneration associated to cardiovascular disease, *Front. Cell Dev. Biol.* 8 (2020) 53.
- [58] E.W. Kostuk, J. Cai, L. Iacovitti, Subregional differences in astrocytes underlie selective neurodegeneration or protection in Parkinson's disease models in culture, *Glia* 67 (8) (2019) 1542–1557.
- [59] C. de Jong, H.J. Gabius, W. Baron, The emerging role of galectins in (re)myelination and its potential for developing new approaches to treat multiple sclerosis, *Cell. Mol. Life Sci.* 77 (7) (2020) 1289–1317.
- [60] G.N. Armaiz-Pena, et al., Adrenergic regulation of monocyte chemoattractant protein 1 leads to enhanced macrophage recruitment and ovarian carcinoma growth, *Oncotarget* 6 (6) (2015) 4266–4273.
- [61] C.E. Olingy, H.Q. Dinh, C.C. Hedrick, Monocyte heterogeneity and functions in cancer, *J. Leukoc. Biol.* 106 (2) (2019) 309–322.
- [62] C. Chester, et al., Immunotherapeutic approaches to ovarian cancer treatment, *J. Immunother. Cancer* 3 (2015) 7.
- [63] D. Payen, et al., Assessment of immunological status in the critically ill, *Minerva Anestesiol.* 66 (10) (2000) 757–763.
- [64] K. Kubler, et al., HLA-class II haplotype associations with ovarian cancer, *Int. J. Cancer* 119 (12) (2006) 2980–2985.
- [65] K. Claes, et al., BRCA1 and BRCA2 germline mutation spectrum and frequencies in Belgian breast/ovarian cancer families, *Br. J. Cancer* 90 (6) (2004) 1244–1251.
- [66] H. Bronger, Immunology and immune checkpoint inhibition in ovarian cancer - current aspects, *Geburtshilfe Frauenheilkd* 81 (10) (2021) 1128–1144.
- [67] P. Jiang, et al., Signatures of T cell dysfunction and exclusion predict cancer immunotherapy response, *Nat. Med.* 24 (10) (2018) 1550–1558.
- [68] Y. Saini, J. Chen, S. Patial, The tristetraprolin family of RNA-binding proteins in cancer: progress and future prospects, *Cancers* 12 (6) (2020).
- [69] F.M. Suk, et al., ZFP36L1 and ZFP36L2 inhibit cell proliferation in a cyclin D-dependent and p53-independent manner, *Sci. Rep.* 8 (1) (2018) 2742.
- [70] M.A. Earp, et al., Genome-wide association study of subtype-specific epithelial ovarian cancer risk alleles using pooled DNA, *Hum. Genet.* 133 (5) (2014) 481–497.

- [71] S. Chandrasekaran, D. Bonchev, Network analysis of human post-mortem microarrays reveals novel genes, microRNAs, and mechanistic scenarios of potential importance in fighting huntington's disease, *Comput. Struct. Biotechnol. J.* 14 (2016) 117–130.
- [72] F. Ponten, K. Jirstrom, M. Uhlen, The human protein atlas—a tool for pathology, *J. Pathol.* 216 (4) (2008) 387–393.
- [73] J. Shin, A. Nile, J.W. Oh, Role of adaptin protein complexes in intracellular trafficking and their impact on diseases, *Bioengineered* 12 (1) (2021) 8259–8278.
- [74] P. Cacciagli, et al., AP1S2 is mutated in X-linked Dandy-Walker malformation with intellectual disability, basal ganglia disease and seizures (Pettigrew syndrome), *Eur. J. Hum. Genet.* 22 (3) (2014) 363–368.
- [75] S. Pan, et al., Pan-cancer landscape of the RUNX protein family reveals their potential as carcinogenic biomarkers and the mechanisms underlying their action, *J Transl Int Med* 10 (2) (2022) 156–174.
- [76] J. Xie, et al., Advances in artificial intelligence to predict cancer immunotherapy efficacy, *Front. Immunol.* 13 (2022), 1076883.